Statistical Characterization and Modeling of Indoor RF-EMF Down-Link Exposure

Biruk Ashenafi Mulugeta, Shanshan Wang, Wassim Ben Chikha, Jiang Liu, Christophe Roblin, Joe Wiart

MDPI

Article

Statistical Characterization and Modelling of Indoor RF-EMF Downlink Exposure

Biruk Ashenafi MULUGETA[1], Shanshan WANG[1], Member, IEEE, Wassim BEN CHIKHA[1], Jiang LIU[1], Christophe ROBLIN[1], Member, IEEE and Joe WIART[1], Senior Member, IEEE

[1] Chaire C2M, LTCI, Telecom Paris, Institut Polytechnique de Paris, France; biruk.mulugeta, shanshan.wang, wassim.benchikha, jiang.liu, joe.wiart@telecom-paris.fr

Abstract: With the increasing use of wireless communication systems, assessment of exposure to radio-frequency electromagnetic field (RF-EMF) has now become very important due to the rise of public risk perception. Since people spend more than 70% of their daily time in indoor environments, including home, office and car, the efforts devoted to indoor RF-EMF exposure assessment has also been increased. However, assessment of indoor exposure to RF-EMF using a deterministic approach is challenging and time consuming task as it is affected by uncertainties due to the complexity of the indoor environment and furniture structure, temporal variability of exposure, existence of many obstructions with unknown dielectric properties, existence of uncontrolled factors that can influence the indoor exposure such as the constant movement of people, random positioning of furniture and doors as people are working in the building, and existence of multiple reflection, refraction, diffraction and scattering. In this study, a statistical approach is used to characterize and model the indoor RF-EMF downlink (DL) exposure. Measurements were conducted in three buildings that are located within a few hundred meters vicinity of two base station sites supporting several cellular antennas (2G, 3G, 4G and 5G). We apply the one-sample Kolmogorov–Smirnov test on the measurement data, and we prove that the indoor RF-EMF DL exposure on each floor over 30 m (length of a wing) is a random process governed by a Gaussian distribution. We validate this using leave-one-out cross validation technique. Consequently, we conclude that the indoor RF-EMF DL exposure on each floor over length of a wing can be modelled by a Gaussian distribution and, therefore, can be characterized by the mean and the standard deviation parameters. Those parameters are mainly influenced by the distance to the base station, the number and type of walls, the orientation of the indoor environment with the azimuth of the base station antenna and floor level.

Keywords: Indoor, Exposure, RF-EMF, Measurement, Kolmogorov–Smirnov, Statistics, Downlink.

Citation: Biruk Ashenafi MULUGETA, Shanshan WANG, Wassim BEN CHIKHA, Jiang LIU and Joe WIART MULUGETA, B.A.; WANG, S.; BEN CHIKHA, W.; LIU, J.; WIART, J. Title. *Sensors* **2022**, *1*, 0.

Received:
Accepted:
Published:

1. Introduction

Since the last decade, radio technologies have undergone a rapid evolution to fulfill the growing needs to connect virtually everyone and everything together, including machines, devices and objects. With this increasing use of wireless communication systems and connected objects, the question of the health impact of radio-frequency (RF) waves and its perception has arisen. Indeed, despite the increasing use and weak exposure, the concern related to electro-magnetic field (EMF) exposure is important [1]. International guidelines, such as ICNIRP [2] and IEEE C95.1 [3], have been established to avoid over exposure that can induce health impacts.

People spend more than 70% of their daily time indoor [4,5]. The power level attenuation can reach up to 20 dB when electromagnetic (EM) wave propagates from outdoor to indoor [6]. When there is high power attenuation from outdoor to indoor, indoor antennas are installed in some indoor environments to enhance the indoor coverage and reduce the user equipment (UE) power consumption as the transmitted power from the UE will be reduced by the up-link power control scheme.

Indoor environments are more densely populated by obstructions such as furniture, walls, floors and partitions of different materials and open spaces such as windows and doors. These obstructions determine the way in which electromagnetic waves propagate along specific paths. Because of the existence of these obstructions in an indoor environment, EM waves suffer from multiple attenuation, reflection, refraction, diffraction and scattering which make the deterministic assessment of indoor RF-EMF exposure challenging and time-consuming task.

Several studies aimed to estimate the indoor RF-EMF exposure in the frequency range of 10 MHz to 6 GHz [7–13]. The most accurate method to estimate the indoor RF-EMF exposure is by directly solving the Maxwell's equations using full wave deterministic techniques, but they are inappropriate for large indoor environment as they require detailed information about the environment which induces memory load and high computational cost [7–9]. For large indoor environment, ray tracing and ray launching deterministic techniques offer a good approximation with lower computational cost [10–12]. However, it is very difficult to utilize these deterministic approaches for the assessment of indoor RF-EMF exposure if the indoor environment is not stable and the dielectric properties and geometry of all obstructions are unknown. In this sense, statistical approaches provide a good approximation.

In this paper, a statistical approach is utilized to characterize and model indoor RF-EMF down-link (DL) exposure. Measurements were conducted in the corridors and some offices of three buildings. The access to these buildings, which are located in Les Clayes sous Bois, has been authorised by ATOS. The buildings, which are shown in Figure 3, are located within a few hundred meters vicinity of two base station sites supporting several cellular antennas (2G, 3G, 4G and 5G) of four operators. First, the contribution of each band to the total exposure is investigated to identify the base stations that generate the incident field. Next, the one-sample Kolmogorov–Smirnov (K-S) test is applied on the measurement data to check if the indoor RF-EMF DL exposure on each floor over 30 m (length of a wing) is a random process governed by a Gaussian distribution. Next, the model is cross checked using the leave-one cross validation technique to check if the distribution is still governed by the same statistical law when we leave one measurement point out. Finally, factors influencing the parameters that determine the RF-EMF DL exposure distribution in the indoor environment are investigated.

The remainder of this paper is organized as follows; we describe the material and method in Section 2. In Section 3, we analyzed the results. Finally, we conclude this paper with Section 4.

2. Material and Method

2.1. Frequency Selective Measurement System

The frequency selective measurement system used in this study consists of a Tektronix RSA306B real-time spectrum analyzer, switch, Arduino-based hardware, tri-axis electric field (E-field) probe and a PC that runs Tektronix SignalVu-PC™ RF signal analysis software and a graphical user interface (GUI) to control the measurements as shown in Figure 1.

The tri-axis E-field probe, which is commercialized by Microwave Vision Group (MVG) as TAS-1208-01 antenna, is used to conduct measurement of RF-EMF exposure on the three orthogonal polarizations (X, Y, and Z). Our frequency selective measurement system allows measurements from 9 kHz to 6.2 GHz. The RF switch connects the spectrum analyzer and the tri-axis E-field probe to conduct measurements on the three orthogonal polarizations.

We will have only a measurement of one selected band at a time if we use only the Tektronix SignalVu-PC™ RF signal analysis software interface. Therefore, we developed a GUI that is synchronized with the SignalVu-PC software to control all measurement parameters and to fetch real-time measurement values. Calibration was performed in the laboratory and an anechoic chamber to maintain the measurement system's accuracy.

The frequency bands, that are under analysis, are the ones used by the network providers in France as given by ANFR [14]. The Resolution Bandwidth (RBW) is set to 250

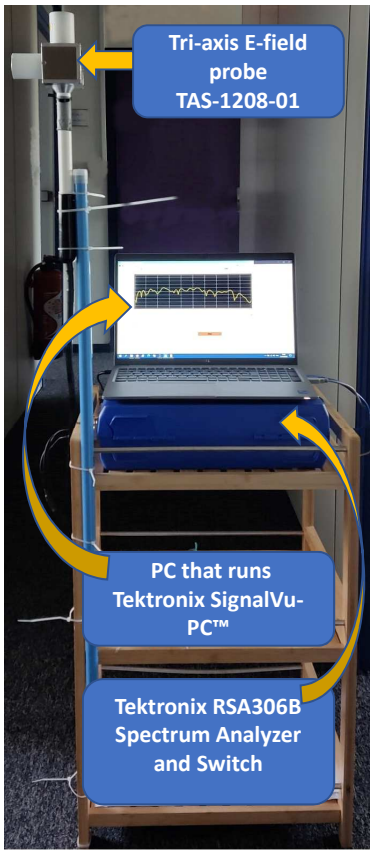

Figure 1. Real-time Spectrum Analyzer EMF measurement system

kHz for for all bands. For each measurement location, the frequency selective measurement system recursively measures the E-field induced by 27 frequency bands (cellular bands used by all network providers in France) on a single axis before switching to the other axes for twenty measurement records. The total E-field is, thus, the root-mean square of the E-field measured on each axis.

A broadband measurement system, which is described in subsection 2.2, has been implemented for the spatial measurements throughout the three buildings as it takes one and fifteen minutes to conduct measurements at a given location using broadband and frequency selective measurement systems, respectively.

2.2. Broadband Measurement System

The broadband measurement system used in this study is commercialized by Narda as NBM-550 broadband field meter with isotropic EF0691 probe as shown in Figure 2. The probe detects electric fields from 100 kHz to 6 GHz.

At a given measurement location, one hundred broadband measurements were recorded in one minute as the broadband measurement system records the RF-EMF DL exposure every 0.6 second.

2.3. Measurement Procedure Description

Measurements were conducted at two different probe heights (1.2m and 1.7m). In total, 1080 spatial measurements were conducted in the corridors of all buildings (30 measurement locations x 2 heights x 3 floors x 2 wings x 3 buildings) with one meter separation distance to investigate the statistical law governing the exposure distribution in the indoor environment as it is necessary to estimate the exposure level as a function of the spatial distribution of the measurements [15]. Besides, 96 spatial measurements (16 measurement points x 2 heights x 1 floors x 1 wings x 3 buildings) were also conducted

Figure 2. NBM-550 broadband measurement system

in the offices on the second floor of one wing of each building (A2R, B2L, and C2L). The ground, first and second floors are labeled 0, 1, and 2, respectively, in between the labels of each wing (for example, the first floor of AR is labeled A1R). The internal walls of buildings A, B, and C are metal, plaster, and metal, respectively. We also conducted frequency selective measurements within the building to identify the antenna that generates the incident field.

Measurements exhibit variations in both spatial and time domains due to radio channel and traffic variations [16]. Radio channel quality varies by the distance to the base station, random environmental variation, and interference variation. Whereas traffic pattern varies by user demand and server load. It is, therefore, important to have an appropriate measurement strategy that takes the scope of such variations into account and removes the dynamics of mobile data traffic from the spatial measurements. Temporal measurement was launched at a stationary position in an office, which is in line of sight (LOS) with the base stations, of one of the buildings to monitor the time variations linked with the traffic change over time. The temporal measurement is used for normalization of the spatial measurements that depend on both location and traffic.

2.4. Field Strength Normalization

In the use of wireless communication, the traffic has an influence on the field emitted by the base station. Since the measurement time of each measurement point is different, the traffic is also different. In this study, we are interested in analyzing the spatial variation of broadband measurements. Therefore, the traffic variation has to be taken into consideration and the measurements should be transformed into their equivalent form at the same reference time. Otherwise, it is difficult to identify the cause of measurement variations as the measurement value is affected by both spatial and temporal variations.

$$\mathbf{E_{t_{i\_eq}}}(t_{i=1}) = \mathbf{E}(t_i) * \frac{\mathbf{E_{ref}}(t_{i=1})}{\mathbf{E_{ref}}(t_i)} \tag{1}$$

The time for the first measurement point, denoted by $t_{i=1}$, was chosen as a reference time. The temporal measurement is, then, extracted for each spatial measurement point based on the time of measurement. After extracting the reference temporal measurement

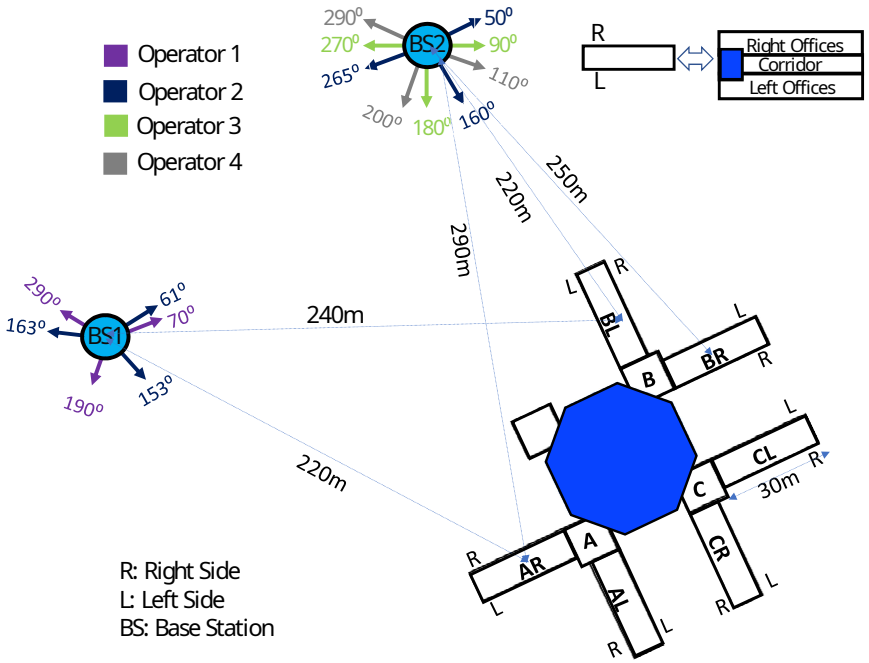

Figure 3. Orientation of buildings with respect to the base stations

($\mathbf{E_{ref}}(\mathbf{t_i})$) for each measurement point, the field measured at a given measurement point "i" has to be weighted by a correction factor of $\frac{\mathbf{E_{ref}}(t_{i=1})}{\mathbf{E_{ref}}(t_i)}$ in order to transform in to its equivalent form at "$t_{i=1}$" ($\mathbf{E_{t_i\_eq}}(t_{i=1})$) [17]. The whole spatial measurements are transformed to their equivalent form at the time of the first measurement point ($\mathbf{E_{i\_eq}}(t_{i=1})$) based on equation (1).

2.5. K-S Test for RF-EMF DL Exposure Statistical Modelling

In this subsection, we describe how to use a statistical approach to characterize indoor RF-EMF DL exposure. We use the measurement data to test and validate a null hypothesis (i.e., the indoor RF-EMF DL exposure is a random process governed by Gaussian distribution over the length of a wing when the indoor environment is located within a few hundred meters vicinity of base station sites) using the one-sample K-S test. K-S test is a non-parametric test that can be used to compare a sample with a reference probability distribution.

The K-S test statistic quantifies the distance between the empirical distribution function of the sample and the cumulative distribution function of the reference distribution. Whereas, p-values (probability values) are often interpreted as the risk of rejecting the null hypothesis of the test when the null hypothesis is actually true [18]. This probability reflects the measure of evidence against the null hypothesis. Small p-values (less than the significance level which is 0.05 in our case) correspond to strong evidence against the null hypothesis. If the p-value is greater than the significance level, then we fail to reject the null hypothesis.

3. Result and Discussion

3.1. Time Variation of Electric Field

As explained in subsection 2.3, we use the reference temporal measurement to record the time variation linked to the traffic change over time. We use this temporal measurement to normalize the spatial measurements as shown in Equation (1). In Figure 4, we plot the temporal variation of electric field over 24 hours averaged per minute and per hour. As

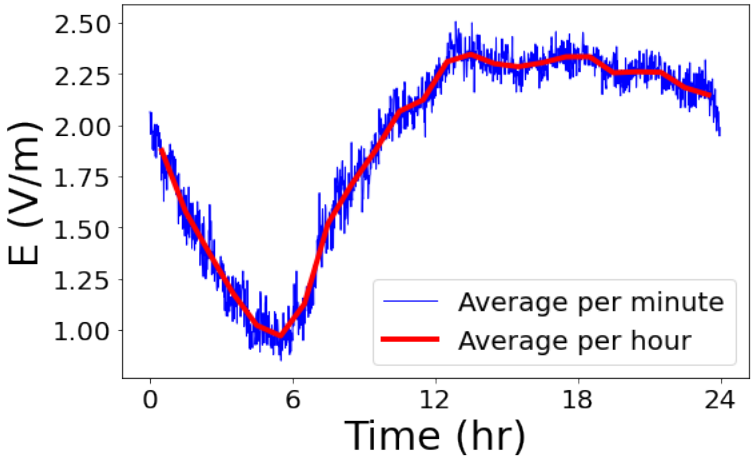

Figure 4. Time variation of electric field in 24 hours

seen from this result, the RF-EMF DL exposure level decreases at night and then increases during the daytime due to the significant increase of cellular usage.

3.2. Frequency Selective Measurement

The base stations, which are located within the vicinity of the buildings, support several cellular antennas on the 700 MHz, 800 MHz, 900 MHz, 1800 MHz, 2100 MHz, 2600 MHz, and 3500 MHz frequency bands for mobile communications. Of the new generation technologies, 5G operates on multiple bands (700 MHz, 2100 MHz and 3500 MHz) and LTE operates on all bands except 900 MHz and 3500 MHz bands [4]. Whereas, 2G and 3G operate on 900 MHz band as shown in Table 1 [14].

Table 1. Mobile communications inter-technology frequency sharing

Band	Technology
700	4G, 5G
800	4G
900	2G, 3G
1800	4G
2100	3G, 4G, 5G
2600	4G
3500	5G

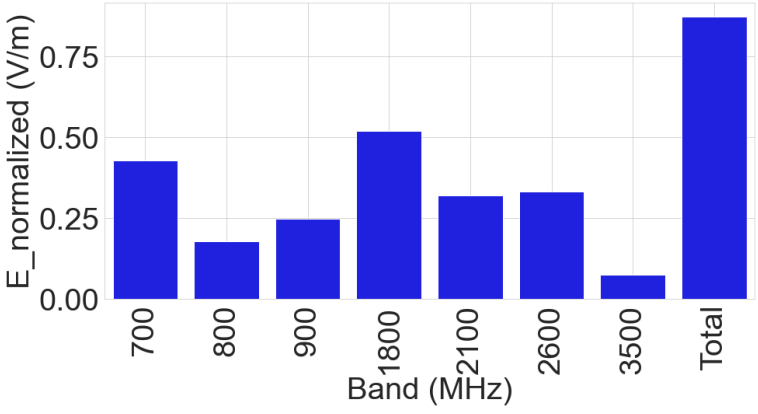

Figure 5. Mean contribution of each band on total **E** field

The result of the frequency selective measurements performed within the building is shown in Figure 5. It validates that the incident fields are generated from the two nearest

base stations as the bands contributing to the total exposure are coherent with frequency bands listed on Cartoradio [14]. Furthermore, it shows that the 700 MHz and 1800 MHz bands dominate the trend of the total exposure, where the total electric field is computed using Equation (2).

$$\mathbf{E_{total}} = \sqrt{\sum_{i \in f} \mathbf{E_i}^2} \tag{2}$$

where $f = \{700MHz, 800MHz, 900MHz, 1800MHz, 2100MHz, 2600MHz, 3500MHz\}$

3.3. Broadband Measurement

Figure 6 shows the variability of the broadband measurement over one minute at a given measurement point.

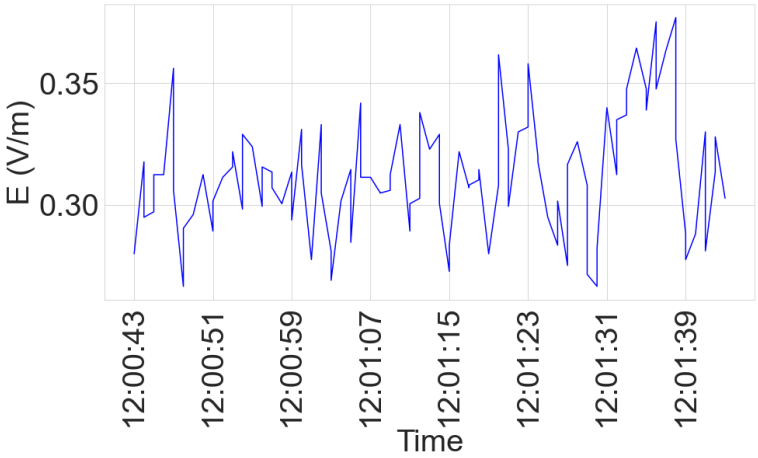

Figure 6. Narda measurement variability over one minute

The analysis in the subsequent sections takes the mean of measurements performed in one-minute for a given measurement point. Therefore, uncertainties are introduced in our measurement analysis due to the variation over one minute.

3.4. Different Probe Height Measurements

The mean and standard deviation of the two measurement heights (1.2m and 1.7m) on all wings of the buildings are listed in Tables 2, 3 and 4 for building A, B and C, respectively.

Table 2. Mean, median and standard deviation of two height measurements for building A

Wing	Type	Height (m)	Mean (V/m)	Median (V/m)	Std (V/m)
A0R	Corridor	1.2	0.753	0.776	0.385
		1.7	0.680	0.687	0.326
A0L	Corridor	1.2	0.313	0.277	0.126
		1.7	0.275	0.238	0.102
A1R	Corridor	1.2	0.922	0.764	0.495
		1.7	0.747	0.632	0.375
A1L	Corridor	1.2	0.417	0.429	0.124
		1.7	0.439	0.429	0.148
A2R	Corridor	1.2	1.104	1.100	0.398
		1.7	1.051	1.031	0.373
	R Office	1.2	1.956	2.028	0.674
		1.7	1.947	2.001	0.724
	L Office	1.2	0.526	0.565	0.197
		1.7	0.515	0.544	0.209
A2L	Corridor	1.2	0.202	0.193	0.052
		1.7	0.246	0.236	0.081

Table 3. Mean, median and standard deviation of two height measurements for building B

Wing	Type	Height (m)	Mean (V/m)	Median (V/m)	Std (V/m)
B0R	Corridor	1.2	0.843	0.715	0.346
		1.7	0.766	0.753	0.249
B0L	Corridor	1.2	0.420	0.431	0.056
		1.7	0.401	0.417	0.081
B1R	Corridor	1.2	0.866	0.842	0.174
		1.7	0.722	0.707	0.156
B1L	Corridor	1.2	0.591	0.579	0.088
		1.7	0.532	0.526	0.073
B2R	Corridor	1.2	1.812	1.729	0.419
		1.7	1.461	1.442	0.214
B2L	Corridor	1.2	0.691	0.705	0.106
		1.7	0.660	0.670	0.112
	R Office	1.2	1.155	0.930	0.495
		1.7	1.056	0.917	0.342
	L Office	1.2	0.804	0.827	0.132
		1.7	0.797	0.768	0.105

Table 4. Mean, median and standard deviation of two height measurements for building C

Wing	Type	Height (m)	Mean (V/m)	Median (V/m)	Std (V/m)
C0R	Corridor	1.2	0.246	0.252	0.035
		1.7	0.26	0.244	0.049
C0L	Corridor	1.2	0.264	0.246	0.098
		1.7	0.254	0.231	0.093
C1R	Corridor	1.2	0.254	0.249	0.066
		1.7	0.268	0.234	0.085
C1L	Corridor	1.2	0.268	0.273	0.055
		1.7	0.271	0.266	0.059
C2R	Corridor	1.2	0.199	0.193	0.040
		1.7	0.224	0.217	0.048
C2L	Corridor	1.2	0.455	0.491	0.152
		1.7	0.365	0.348	0.106
	R Office	1.2	0.335	0.263	0.14
		1.7	0.312	0.277	0.104
	L Office	1.2	0.790	0.781	0.151
		1.7	0.911	0.926	0.186

In Table 5, we compute the correlation coefficients between the statistical parameters (i.e. mean, median and standard deviation) of the two probe heights according to the values presented in the Table 2, 3 and 4 for the buildings A, B and C, respectively. As seen from these results, the correlation coefficients on each building are close to one. Hence, the measurements at the two probe heights are highly correlated in terms of mean, median and standard deviation. Consequently, we can consider that the exposure level for these two heights are similar. In this case, we merge the measurements at the two probe heights for the subsequent measurement analysis.

Table 5. Correlation coefficients between the measurements performed at the two probe heights

Building	Correlation Coefficient		
	Mean	Median	Std
A	0.993	0.996	0.966
B	0.990	0.985	0.956
C	0.974	0.982	0.836

3.5. Statistical Analysis of Measurements

In order to characterize the indoor RF-EMF DL exposure in different building's corridors, we apply the one-sample K-S test, which is described in subsection 2.5. Under the null hypothesis (i.e., that the indoor RF-EMF DL exposure is a random process governed by a Gaussian distribution at each wing), we find out that the p-values on all floors of the three buildings are greater than 0.05 as shown in Table 6. This proves the null hypothesis by not rejecting it with 0.05 significance level and 95% confidence level, which shows the percentage of times we expect to get close to the same estimate if we run our experiment again. Besides, the correlation coefficients between the mean and the median are 0.995, 0.985 and 0.995 of the three buildings A, B and C, respectively. Therefore, we can conclude that the indoor RF-EMF DL exposure on each floor over the length of a wing can be modelled as a random process governed by a Gaussian distribution at each wing that is located within a few hundred meters vicinity of base stations sites. In other words, the incident field on each floor is almost constant over the length of a wing.

Table 6. K-S Test checking the normality of exposure on all wings of building A, B and C

Wing	Type	Test Statistic	p-value
A0R	Corridor	0.118	0.308
A0L	Corridor	0.133	0.187
A1R	Corridor	0.147	0.086
A1L	Corridor	0.08	0.795
A2R	Corridor	0.089	0.599
	R Office	0.144	0.848
	L Office	0.166	0.776
A2L	Corridor	0.114	0.363
B0R	Corridor	0.131	0.287
B0L	Corridor	0.139	0.244
B1R	Corridor	0.12	0.365
B1L	Corridor	0.085	0.814
B2R	Corridor	0.173	0.062
B2L	Corridor	0.138	0.25
	R Office	0.248	0.235
	L Office	0.114	0.932
C0R	Corridor	0.091	0.991
C0L	Corridor	0.173	0.078
C1R	Corridor	0.104	0.507
C1L	Corridor	0.089	0.656
C2R	Corridor	0.106	0.498
C2L	Corridor	0.162	0.056
	R Office	0.251	0.172
	L Office	0.130	0.916

Accordingly, we can model the indoor RF-EMF DL exposure on each floor over the length of a wing using a Gaussian distribution and characterize it by only the mean and standard deviation parameters. To confirm this result, we perform the leave-one-out cross-validation technique in the next subsection.

3.6. Leave-One-Out Cross-Validation

In this subsection, we cross-check the validity of our model using the leave-one-out cross-validation technique. K-S test is used to check the normality of the distribution of the wings by leaving one measurement point out at a time in an iterative way for all measurement points of wings on each floor. Then, we statistically prove that indoor RF-EMF DL exposure on each floor over the length of a wing is governed by Gaussian distribution with a probability of 0.973.

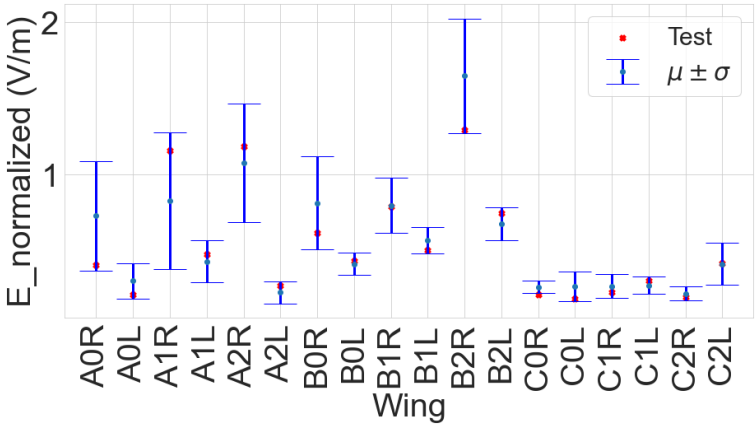

Figure 7. Validation of test point within one standard error from the mean in the corridors of all buildings

In Figure 7, uncertainties on error bar plots are shown to indicate where randomly chosen test data from N measurement data points will fall within one standard deviation from the mean of the rest (N-1) measurement data points. The random test point, which is not considered in the calculation of the mean and the standard deviation, falls within one, two and three standard errors from the mean with a probability of 0.74, 0.95 and 0.99, respectively.

3.7. Factors Influencing the Mean Indoor RF-EMF DL Exposure

The indoor RF-EMF DL exposure level is dependent on the distance to the base station, the number and type of walls, the orientation of the indoor environment with the azimuth of the base station antenna and floor level. In this subsection, we will analyze the influence these factors on the mean of the three building wings on each floor.

Table 7. Mean and standard deviation of measurements in A, B and C wings

Wing	Type	μ (V/m)	σ (V/m)	σ/μ
A0R	Corridor	0.716	0.361	0.5
A0L	Corridor	0.294	0.117	0.4
A1R	Corridor	0.834	0.451	0.5
A1L	Corridor	0.428	0.138	0.3
A2R	Corridor	1.077	0.389	0.4
	R Office	1.951	0.722	0.4
	L Office	0.521	0.211	0.4
A2L	Corridor	0.224	0.072	0.3
B0R	Corridor	0.804	0.307	0.4
B0L	Corridor	0.411	0.071	0.2
B1R	Corridor	0.793	0.182	0.2
B1L	Corridor	0.562	0.087	0.2
B2R	Corridor	1.636	0.38	0.2
B2L	Corridor	0.675	0.111	0.2
	R Office	1.105	0.442	0.4
	L Office	0.801	0.122	0.2
C0R	Corridor	0.253	0.045	0.2
C0L	Corridor	0.259	0.096	0.4
C1R	Corridor	0.261	0.077	0.3
C1L	Corridor	0.270	0.057	0.2
C2R	Corridor	0.212	0.046	0.2
C2L	Corridor	0.410	0.139	0.3
	R Office	0.324	0.127	0.4
	L Office	0.851	0.186	0.2

The orientations of the wings determine the slight angle from the azimuth of base station antennas and their LOS positioning to the base stations. Thus, orientation of the wings in turn determines the antenna gain which reduces with an increase of the angle in going to the right and left beyond the peak of the main beam. Antenna is also working outside its main beam, but with less gain than the declared maximum gain.

The mean exposure levels on the AL and AR wings of building A are 0.315 V/m and 0.876 V/m, respectively. The mean exposure levels on the BL and BR wings of building B are 0.55 V/m and 1.08 V/m, respectively. The mean exposure levels on the CL and CR wings of building C are 0.24 V/m and 0.31 V/m, respectively. In building A corridors, the ratio of the mean exposure level on AR to that of AL (8.87 dB) is higher than the corresponding ratio on building B corridors (5.85 dB) and building C corridors (2.24 dB). It makes complete sense to have a lower exposure level difference between the two wings of building B as both wings are in LOS with the base stations in contrary to building A whose left wing is in non-LOS (NLOS) with the base stations. Building C has the lowest

mean exposure level difference between its wings as both wings are in NLOS with the base stations.

We can also see the effect of orientation on building B exposure since BL is in LOS with both base stations, but the contribution of exposure from BS1 should be higher as the incident field from BS2 encounters higher attenuation by passing through multiple walls from the rear end of the wing since the axis of the wing is parallel to the direction of LOS to BS2. We expect higher exposure level on wing BL as the distance to the base station is lower compared to wing BR, but ratio of the mean exposure level on wing BR to that of BL is 5.85 dB. The mean exposure level on wing BR is higher than that of BL due to the fact that the wing BR has a lower slight angle from the azimuth of the antenna than that of BL due to its orientation. As the exposure level depends on the azimuth of the antenna and the antenna gain decreases away from the direction of the main beam, a higher exposure level on BR than BL is acceptable.

As listed in Table 7, the wings AR and BR have higher exposure levels than the other wings of the three buildings. When we compare the exposure level on the two wings, we can see that the ratio of the mean exposure level on wing BR to that of AR is 1.8 dB even though AR is closer to the base station. If distance was the only factor that determines the exposure level, AR should have a higher exposure level. But, the mean exposure level on wing BR is higher than that of AR due to the fact that the slight angle of BR from the azimuth of the antenna is lower than that of AR because of their orientation. The ratio of the mean exposure level on AR to that of BL is 4.1 dB due to its lower slight angle from the azimuth of the antenna even though BL is closer to the base station. Therefore, the orientation of the wing influences the exposure level as it determines the slight angle from the azimuth of the antenna and its LOS positioning to the base station.

Table 8. Comparison of corridor exposure level with the left and right side offices of A2R, B2L and C2L

Wing	Mean (V/m)		
	Left Office	**Corridor**	**Right Office**
A2R	0.52	1.08	1.95
B2L	0.80	0.68	1.11
C2L	0.85	0.41	0.32

The two base stations are exposing AR from the right side of the wing, so that we can clearly see the effect of the wall as the incident field is coming from one direction. Table 8 shows the influence of wall on indoor exposure. The first wall layer is the wall between the corridor and the offices which are in LOS with the base station. Whereas, the second wall layer is the wall between the corridor and offices which are in NLOS with the base station. The incident field has to pass through the first and second wall layers in order to reach the corridor and offices, respectively, that are in NLOS with the base station. We expect lower exposure level when the incident field passes through each layer of walls due to wall attenuation as shown in Table 8. For A2R, the ratio of the mean exposure level on the right side to that of the left side of the first and second wall layers are 5.16 dB and 6.31 dB, respectively. This is mainly due to the wall attenuation on the first and second wall layers. The ratio on the second wall layer (between the corridor and the left offices) is higher. This makes complete sense as some portion of the field propagates through the corridor instead of passing through the wall layer into the left-side offices. That is why the two-layer have different percentage change even though they have the same wall type. For B2L, the ratio of the mean exposure level on the right side offices to that of the corridor and the mean exposure level on the corridor to that of the left side offices are 4.28 dB and -1.49 dB, respectively. It seems weird that the exposure level in the corridor is lower than the offices on both sides, but it makes complete sense as the incident field propagates toward BL from both sides of the wing. It is difficult to see the effect of the wall on C2L, since it is in NLOS with the base stations.

The ratio of the mean exposure level on the right side to that of the left side of the first and second wall layers in B2L is lower compared to that of A2R due to the existence of different type of walls in the two buildings as the internal walls of building A and B are metal and plaster, respectively. Metal walls have higher attenuation than plaster walls due to their shielding effect. Therefore, the exposure level is influenced by the type and the number of walls the incident field encounters.

$$\theta_{geo} = arctan(\frac{H_{BS} - h_{mes}}{d}) \tag{3}$$

Furthermore, the indoor RF-EMF DL exposure is influenced by the floor level of a building [19,20]. The floor level of a building determines the beam down tilt angle which in turn determines the antenna gain. The antenna gain reduces with an increase of the angle in going up and down beyond the peak of the main beam. The beam down tilt angle depends on geometrical factor (θ_{geo}) which takes into account the average height difference between the base station (H_{BS}) and measurement antenna height (h_{mes}) as well as the distance to the base station (d) as shown in Equation 3 [21,22]. We can consider wings (AR, BR and BL) that are in LOS with the base station antennas in order to see the influence of floor level on an indoor RF-EMF DL exposure level. But, the orientation of BS2 with BL and NLOS positioning of BR to BS1 makes it difficult to clearly see the influence of floor level on BL and BR wings. Since AR has a clear LOS orientation with both base stations, it will give us a clear view of floor level influence on the indoor RF-EMF DL exposure. The mean exposure level on the ground, first and second floors are 0.716 V/m, 0.834 V/m and 1.077 V/m, respectively. In AR, the ratios of the mean exposure level on second floor to first floor and first floor to ground floor are 2.22 dB and 1.33 dB, respectively. This implies that the indoor RF-EMF DL exposure gets higher with an increase in floor level. The measurement antenna height increases by three meters with the floor level as the the height of each floor is three meter. The beam angle difference between each floor level will get smaller as θ_{geo} gets lower when d gets higher based on Equation 3. That is why the influence of floor level on indoor RF-EMF DL exposure is less compared to the other factors (orientation and wall) as ATOS is located a few hundred meters away from the base station sites.

4. Conclusion

This paper analyzes RF-EMF DL exposure inside buildings having cellular antennas located at more than 200 meters from the buildings. In the three buildings, 1176 measurements have been performed with a broadband probe at different wings and floors. With the base station antenna far away, the exposure is well below 1% of the ICNIRP reference levels as expected.

A statistical approach has been implemented to characterize and model indoor RF-EMF DL exposure. The measurement data performed in all the corridor were analyzed and the p-values of the one-sample K-S test are above 0.05. Therefore, it has been statistically proved that the indoor RF-EMF DL exposure on each floor over the length of a wing can be modeled by a Gaussian distribution when the size of the building is small compared to the distance to the base station antennas. In such case, the the mean and the standard deviation characterize the RF-EMF DL exposure distribution in the indoor environment. These parameters are influenced by the number and type of walls, the orientation of the indoor environment with the azimuth of the base station antenna and floor level.

Finally, the result of this work can be used as a step-stone to install a global indoor RF-EMF DL exposure monitoring system in ATOS via the implementation of measurements carried out by RF sensors distributed in the buildings.

Author Contributions: Conceptualization, B.A.M. and J.W.; methodology, B.A.M. and J.W.; software, B.A.M.; validation, B.A.M. and J.W.; formal analysis, B.A.M.; data curation, B.A.M.; writing—original draft preparation, B.A.M.; writing—review and editing, J.W., C.R., S.W, W.B.C. and J.L.; visualization, B.A.M.; supervision, J.W. and C.R.; All authors have read and agreed to the published version of the manuscript.

Institutional Review Board Statement: All procedures performed in studies involving human participants were in accordance with the ethical standards of the institutional and/or national research committee and with the 1964 Helsinki declaration and its later amendments or comparable ethical standards.

Informed Consent Statement: Informed consent was obtained from all subjects involved in the study.

Data Availability Statement: The data presented in this study are available on request from the corresponding author.

Acknowledgments: The authors would like to acknowledge ATOS and in particular Mr Quintin and Duluc that have allowed the measurements in the ATOS facilities.

Conflicts of Interest: The authors declare no conflict of interest.

Abbreviations

The following abbreviations are used in this manuscript:

RF	Radio Frequency
EMF	Electro-Magnetic Field
DL	Down-Link
ICNIRP	International Commission on Non-Ionizing Radiation Protection
IEEE	Institute of Electrical and Electronics Engineers
UE	User Equipment
K-S	Kolmogorov–Smirnov
GUI	Graphical User Interface
MVG	Microwave Vision Group
ANFR	L'Agence Nationale des FRéquences
RBW	Resolution Band Width
LOS	Line Of Sight
NLOS	Non Line Of Sight

References

1. Feuardent, J.; Scanff, P.; Crescini, D.; Rannou, A. Occupational external exposure to ionising radiation in France (2005–2011). *Radiation protection dosimetry* **2013**, *157*, 610–618.
2. ICNIRP. The ICNIRP Guidelines for Limiting Exposure to Electromagnetic Fields 100 kHz - 300 GHz. https://www.icnirp.org/en/frequencies/radiofrequency/rf-emf-100-khz-300-ghz.html, 2021. Accessed on 2021-06-19.
3. IEEE Standards Coordinating Committee, .; et al. IEEE standard for safety levels with respect to human exposure to radio frequency electromagnetic fields, 3kHz to 300GHz. *IEEE C95. 1-1991* **1992**.
4. Zeghnoun, A.; Dor, F. Description du Budget Espace Temps et Estimation de Lexposition de la Population Francaise Dans Son Logement. *Institut de Veille Sanitaire: Lyon, France* **2010**.
5. Klepeis, N.E.; Nelson, W.C.; Ott, W.R.; Robinson, J.P.; Tsang, A.M.; Switzer, P.; Behar, J.V.; Hern, S.C.; Engelmann, W.H. The National Human Activity Pattern Survey (NHAPS): a resource for assessing exposure to environmental pollutants. *Journal of Exposure Science & Environmental Epidemiology* **2001**, *11*, 231–252.
6. Schüz, J.; Mann, S. A discussion of potential exposure metrics for use in epidemiological studies on human exposure to radiowaves from mobile phone base stations. *Journal of Exposure Science & Environmental Epidemiology* **2000**, *10*, 600–605.
7. Lee, J.; Lai, A. FDTD analysis of indoor radio propagation. In Proceedings of the IEEE Antennas and Propagation Society International Symposium. 1998 Digest. Antennas: Gateways to the Global Network. Held in conjunction with: USNC/URSI National Radio Science Meeting (Cat. No. 98CH36. IEEE, 1998, Vol. 3, pp. 1664–1667.
8. Laner, A.; Bahr, A.; Wolff, I. FDTD simulations of indoor propagation. In Proceedings of the Proceedings of IEEE Vehicular Technology Conference (VTC). IEEE, 1994, pp. 883–886.
9. El Ahdab, Z.; Akleman, F. An efficient 3-D FDTD-PE hybrid model for radio wave propagation with near-source obstacles. *IEEE Transactions on Antennas and Propagation* **2018**, *67*, 346–355.

10. Aguirre, E.; Arpon, J.; Azpilicueta, L.; Miguel-Bilbao, S.d.; Ramos-Gonzalez, M.V.; Falcone, F.J.; et al. Evaluation of electromagnetic dosimetry of wireless systems in complex indoor scenarios with human body interaction. *Progress In Electromagnetics Research B* **2012**, *43*, 189–209.
11. Aguirre, E.; Arpon, J.; Azpilicueta, L.; Lopez, P.; De Miguel, S.; Ramos, V.; Falcone, F. Estimation of electromagnetic dosimetric values from non-ionizing radiofrequency fields in an indoor commercial airplane environment. *Electromagnetic Biology and Medicine* **2014**, *33*, 252–263.
12. Celaya-Echarri, M.; Azpilicueta, L.; Ramos, V.; Lopez-Iturri, P.; Falcone, F. Empirical and Modeling Approach for Environmental Indoor RF-EMF Assessment in Complex High-Node Density Scenarios: Public Shopping Malls Case Study. *IEEE Access* **2021**, *9*, 46755–46775.
13. Chiaramello, E.; Bonato, M.; Fiocchi, S.; Tognola, G.; Parazzini, M.; Ravazzani, P.; Wiart, J. Radio frequency electromagnetic fields exposure assessment in indoor environments: a review. *International journal of environmental research and public health* **2019**, *16*, 955.
14. ANFR. The map of radio sites and wave measurements. https://www.cartoradio.fr/.
15. De Andrade, H.; De Figuêiredo, A.; Fialho, B.; da S. Paiva, J.; Queiroz Júnior, I.d.S.; Sousa, M. Analysis and development of an electromagnetic exposure map based in spatial interpolation. *Electronics Letters* **2020**, *56*, 373–375.
16. Shawel, B.S.; Mare, E.; Debella, T.T.; Pollin, S.; Woldegebreal, D.H. A Multivariate Approach for Spatiotemporal Mobile Data Traffic Prediction. *Engineering Proceedings* **2022**, *18*, 10.
17. Wiart, J. *Radio-frequency human exposure assessment: from deterministic to stochastic methods*; John Wiley & Sons, 2016.
18. Bevans, R. Understanding P-values. https://www.scribbr.com/statistics/p-value/, 2022. Accessed on 2022-11-03.
19. Anglesio, L.; Benedetto, A.; Bonino, A.; Colla, D.; Martire, F.; Saudino Fusette, S.; d'Amore, G. Population exposure to electromagnetic fields generated by radio base stations: evaluation of the urban background by using provisional model and instrumental measurements. *Radiation protection dosimetry* **2001**, *97*, 355–358.
20. for Non-Ionizing Radiation Protection) Standing Committee on Epidemiology:, I.I.C.; Ahlbom, A.; Green, A.; Kheifets, L.; Savitz, D.; Swerdlow, A. Epidemiology of health effects of radiofrequency exposure. *Environmental health perspectives* **2004**, *112*, 1741–1754.
21. Niemela, J.; Lempiainen, J. Impact of mechanical antenna downtilt on performance of WCDMA cellular network. In Proceedings of the 2004 IEEE 59th Vehicular Technology Conference. VTC 2004-Spring (IEEE Cat. No. 04CH37514). IEEE, 2004, Vol. 4, pp. 2091–2095.
22. Niemelä, J.; Isotalo, T.; Lempiäinen, J. Optimum antenna downtilt angles for macrocellular WCDMA network. *EURASIP Journal on Wireless Communications and Networking* **2005**, *2005*, 1–12.